

Article

# Performance Evaluation of Cluster Validity Indices (CVIs) on Multi/Hyperspectral Remote Sensing Datasets

Huapeng Li <sup>1,\*</sup>, Shuqing Zhang <sup>1</sup>, Xiaohui Ding <sup>1,2</sup>, Ce Zhang <sup>3</sup> and Patricia Dale <sup>4</sup>

<sup>1</sup> Northeast Institute of Geography and Agroecology, Chinese Academy of Sciences, Changchun 130012, China; zhangshuqing@neigae.ac.cn (S.Z.); dingxiaohui@neigae.ac.cn (X.D.)

<sup>2</sup> University of Chinese Academy of Sciences, Beijing 100049, China

<sup>3</sup> Lancaster Environment Centre, Lancaster University, Lancaster LA1 4YQ, UK; cz1a13@soton.ac.uk

<sup>4</sup> Environmental Futures Research Institute, School of Environment, Griffith University, Brisbane, QLD 4111, Australia; p.dale@griffith.edu.au

\* Correspondence: lhpcas@163.com; Tel.: +86-431-8554-2230

Academic Editors: Guoqing Zhou, Qihao Weng and Prasad S. Thenkabail

Received: 21 December 2015; Accepted: 21 March 2016; Published: 30 March 2016

**Abstract:** The number of clusters (*i.e.*, the number of classes) for unsupervised classification has been recognized as an important part of remote sensing image clustering analysis. The number of classes is usually determined by cluster validity indices (CVIs). Although many CVIs have been proposed, few studies have compared and evaluated their effectiveness on remote sensing datasets. In this paper, the performance of 16 representative and commonly-used CVIs was comprehensively tested by applying the fuzzy *c*-means (FCM) algorithm to cluster nine types of remote sensing datasets, including multispectral (QuickBird, Landsat TM, Landsat ETM+, FLC1, and GaoFen-1) and hyperspectral datasets (Hyperion, HYDICE, ROSIS, and AVIRIS). The preliminary experimental results showed that most CVIs, including the commonly used DBI (Davies-Bouldin index) and XBI (Xie-Beni index), were not suitable for remote sensing images (especially for hyperspectral images) due to significant between-cluster overlaps; the only effective index for both multispectral and hyperspectral data sets was the WSJ index (WSJI). Such important conclusions can serve as a guideline for future remote sensing image clustering applications.

**Keywords:** cluster validity index; remote sensing; image clustering; cluster number of image

## 1. Introduction

Land use/cover data is crucial for diverse disciplines (e.g., ecology, geography, and climatology) since it serves as a basis for various “real world” applications [1–3]. Remote sensing technique have become the mainstream means to acquire land use/cover data, owing to its specific advantages, including synoptic views and cost-effectiveness [4,5]. Remote sensing image clustering, which utilizes only the statistical information inherent in the image without human interference, is one of the most widely used methods to produce land cover information [6,7]. It is also valued because of its high efficiency (*i.e.*, it does not use training samples) [8].

The success of clustering (unsupervised classification) depends greatly on the proper determination of cluster number (*i.e.*, the optimal number of classes) [9]: if the number of classes selected is less than the actual number, one or more separate classes would be merged into other classes; conversely, if larger, one or more homogeneous classes would be separated into different classes. The consequence is that the information contained in the raw data is incorrectly explored and used and the classification results will not be coincident with the “real” situation [10]. In this circumstance, the role

of the cluster validity index (CVI), which is designed to detect the optimal cluster number for a given dataset, therefore, becomes critical [11].

Generally, a CVI is comprised of two indicators, namely compactness and separation. Compactness, which indicates the concentration of data points that belong to the same cluster, is usually measured by the distance between each data point and its cluster center [10]: the smaller the distance, the better the compactness of the cluster. Separation, which expresses the degree of isolation among clusters, is usually measured by the distance between cluster centroids: the larger the distance, the stronger the isolation of clusters [12]. Ideally, a dataset is partitioned with high compactness within each cluster and large separation between each pair of clusters. However, the two indicators are often mutually conflicting [13]; with increasing cluster number, the compactness becomes larger while the separation becomes smaller. Therefore, a good balance between the two indicators is required in the design of CVIs. To date, researchers from different disciplines have proposed a large number of CVIs for various types of applications.

In the remote sensing field, CVIs such as the Davies-Bouldin index (DBI) and the Xie-Beni index (XBI) have been widely used in image clustering applications. For example, DBI was employed to evaluate the fitness of candidate clustering by Bandyopadhyay and Maulik [9], and to guide satellite image clustering by Das *et al.* [14]; XBI was used to determine the optimal cluster number of IRS image by Maulik and Saha [15]; and was applied for multi-objective automatic image clustering [16,17]. However, in the absence of systematic and comprehensive evaluation of CVIs for remote sensing applications, CVIs are usually subjectively selected. This means that, without evaluation, they cannot necessarily be relied on. In fact, remote sensing data is well known for its complexity and uncertainty, with the specific characteristics as follows: (1) fuzzy and nonlinear class boundaries; (2) significant overlap among pixels from different classes (the overlap problem) [18]; and (3) high dimensionality and huge quantities of data. An appropriate CVI should, therefore, be designed taking account of these properties of remote sensing data.

To draw some general conclusions, although some efforts have been made to compare or evaluate the performance of CVIs in different environments [10,19–21], little attention has been paid to remote sensing data. Thus, the question remains as to how to select appropriate CVIs for remote sensing image clustering. Such a question can only be answered through an extensive evaluation of CVIs on various types of remote sensing data sets. However, to the best of our knowledge, few studies have addressed this issue. The objective of this paper is to fill that gap and identify one or several CVIs that are generally suitable for remote sensing datasets from a total of sixteen CVIs. The commonly used fuzzy c-means (FCM) and K-means algorithms were applied in this paper to cluster nine types of remote sensing datasets, including five types of multispectral and four types of hyperspectral images. This is of great significance since it can serve as a guideline for future remote sensing image clustering with diverse data types.

The remainder of this paper is organized as follows. In Section 2, the clustering problem and the FCM and K-means algorithms are briefly outlined; the sixteen CVIs evaluated in this paper are reviewed and detailed in Section 3; the experiments and results are provided in Section 4; the results are analyzed and discussed in Section 5; and conclusions are drawn in Section 6.

## 2. The Clustering Problem

In this section, we briefly review the clustering problem and the classical fuzzy c-means algorithm.

### 2.1. The Clustering Problem

Clustering is widely used in many fields to derive information on distributions and patterns in raw data [11]. It aims at partitioning a given data set into groups (clusters) according to a predefined criteria (usually the Euclidean distance) [20]. Let  $X = \{x_1, x_2, \dots, x_N\}$  be a possible given dataset (with  $N$  points), and  $K$  the number of clusters (*i.e.*, patterns) of the data. The purpose of clustering is to evolve a partition matrix  $U(X)$  of the data to determine a partition  $C = \{C_1, C_2, \dots, C_K\}$ , in which the

points in the same cluster are as close (*i.e.*, have high similarity) as possible while those in different clusters are dispersed as far (*i.e.*, have high dissimilarity) as possible. The partition matrix can be denoted as  $U = [\mu_{ij}]$ ,  $1 \leq i \leq K$ ,  $1 \leq j \leq N$ , where  $\mu_{ij}$  is the grade of membership of point  $x_j$  to cluster  $C_i$  ( $i = 1, \dots, K$ ).

Clustering can be performed in two forms: crisp and fuzzy. In crisp clustering, any one point of the given dataset belongs to only one class of clusters, that is  $\mu_{ij} = 1$  if  $x_j \in C_i$ ; otherwise  $\mu_{ij} = 0$ . In fuzzy clustering, a point may belong to several or all classes with a certain grade of membership. In this case, the partition matrix  $U(X)$  is represented as  $U = [\mu_{ij}]$ , where  $\mu_{ij} \in [0, 1]$ . It should be noted that crisp clustering is a special version of fuzzy clustering in which the grade of membership of a point to a cluster is either 0 or 1. Once a fuzzy clustering structure is determined by a specific algorithm, each point of the given data will be assigned to the most likely cluster (*i.e.*, with the largest grade of membership for that point). Through this process, the fuzzy clustering can be transformed into crisp clustering for real applications.

## 2.2. The Fuzzy C-Means Algorithm

The classical fuzzy c-means (FCM) algorithm proposed by Bezdek [22] has been successfully used in a wide domain of applications, such as agricultural engineering, image analysis, and target recognition, among others [20,23,24]. The objective of FCM is to evolve a set of cluster centers through minimizing the weighted within-cluster sum of squared error function  $J_m$ , which is defined as:

$$J_m = \sum_{j=1}^N \sum_{i=1}^K (\mu_{ij})^m \|x_j - z_i\|^2, 0 < \sum_{j=1}^N \mu_{ij} < N, i \in \{1, 2, \dots, K\} \quad (1)$$

where  $Z = (z_1, z_2, \dots, z_K)$  is a group of cluster centers,  $z_i \in R^d$  ( $d$  is the number of features included in each point).  $\|\dots\|$  is a Euclidean norm measuring the similarity between a point and the corresponding cluster center. The weighting exponent  $m$  controls the fuzziness of the grade of membership. The partition matrix  $\mu_{ij}$  and the cluster center set  $Z$  in the function  $J_m$  can be calculated using the following equations:

$$\mu_{ij} = \left[ \sum_{i=1}^K \left( \frac{\|x_j - z_i\|^2}{\|x_j - z_k\|^2} \right)^{1/(m-1)} \right]^{-1}, i \in \{1, 2, \dots, K\}, j \in \{1, 2, \dots, N\} \quad (2)$$

and

$$z_i = \frac{\sum_{j=1}^N (\mu_{ij})^m x_j}{\sum_{j=1}^N (\mu_{ij})^m}, i \in \{1, 2, \dots, K\} \quad (3)$$

The FCM algorithm iteratively searches the fuzzy partition matrix and the cluster centers with a greedy searching strategy, until either no more changes are found in the cluster centers or the differences between two successive cluster centers fall below a predefined threshold. Normally, the FCM algorithm consists of the following steps:

*Step 1:* Determine the number of cluster  $K$  and the weighting exponent  $m$ , initialize the cluster centers  $Z(z_1, z_2, \dots, z_K)$  randomly, and define a threshold of iteration termination  $\varepsilon$ .

*Step 2:* Update the fuzzy partition matrix using Equation (2).

*Step 3:* Recalculate the cluster center set  $Z_{new}$  using Equation (3).

*Step 4:* If  $\|Z_{new} - Z\| \leq \varepsilon$ , stop the iteration and output the clustering result; otherwise, go to step 2.

### 2.3. The K-Means Algorithm

The K-means algorithm is one of the most commonly used methods for unsupervised image classification [2]. Similar to FCM, the objective of K-means is to determine a set of cluster centers through minimizing the clustering metric  $M$ , which is defined as

$$M = \sum_{i=1}^K \sum_{x_j \in C_i} \|x_j - z_i\| \quad (4)$$

where  $C_i$  represents a cluster with  $z_i$  as its cluster center.

A greedy searching strategy is also employed in K-means to search for the optimal set of cluster centers, until a predefined termination condition is met. The main steps of the algorithm are as follows:

*Step 1:* Determine the cluster number  $K$  and the maximum iteration number  $Max\_iter$  to generate the initial cluster centers randomly.

*Step 2:* Assign pixel  $x_j$  to cluster  $C_i$  if  $\|x_j - z_i\| < \|x_j - z_k\|$ ,  $k \in \{1, 2, \dots, K\}$ , and  $i \neq k$ .

*Step 3:* Calculate new cluster center ( $z_i^{new}$ ) for cluster  $C_i$  as  $z_i^{new} = \frac{1}{N_i} \sum_{x_j \in C_i} x_j$ , where  $N_i$  denotes the number of pixels in cluster  $C_i$ .

*Step 4:* If  $Max\_iter$  is reached, terminate the cycle and output the clustering result; otherwise, go to Step 2.

### 3. Cluster Validity Indices (CVIs)

Broadly, current fuzzy CVIs (for fuzzy clustering) can be classified into two forms: one (called simple CVIs) only considers the fuzzy grades of membership to a class of the data (e.g., the partition coefficient), the other (called advanced CVIs) takes both fuzzy grads of membership and the geometrical properties (i.e., the structure) of the original data into account (e.g., the well-known XBI) [10]. In fact, crisp CVIs (for crisp clustering) which only consider the geometrical properties of the original data (e.g., the well-known DBI) are special versions of advanced CVIs, and can also be used in fuzzy image clustering analysis [12]. In this study, a total of 16 representative and commonly used CVIs of different forms were chosen for evaluation, including three simple CVIs, and thirteen advanced CVIs.

It is noteworthy that some CVIs (e.g., XBI) indicate the optimal cluster number of data by using the maximum value, while the others use the minimum value. For convenience, we subsequently denote the former (the larger, the better CVI) as  $CVI^+$ , and the latter (the lower, the better CVI) as  $CVI^-$ .

#### 3.1. Simple CVIs

(1) The partition coefficient ( $PC^+$ ) [25] evaluates the compactness by using the averaged strength of belongingness of data, and is defined as:

$$PC(K) = \frac{1}{N} \sum_{i=1}^K \sum_{j=1}^N \mu_{ij}^2 \quad (5)$$

(2) The partition entropy ( $PE^-$ ) is formed based upon the logarithmic form of  $PC$  [22], and is defined as:

$$PE(K) = -\frac{1}{N} \sum_{i=1}^K \sum_{j=1}^N \mu_{ij} \log_2(u_{ij}) \quad (6)$$

(3) The modification of  $PC$  ( $MPC^+$ ) [26] is designed to reduce the monotonic tendency of  $PC$  and  $PE$ . The index is defined as:

$$MPC(K) = 1 - \frac{K}{K-1}(1 - PC) \quad (7)$$

### 3.2. Advanced CVIs

(1) The Davies-Bouldin Index ( $DBI^-$ ) [27] estimates the ratio of within-cluster compactness to between-cluster separation, which is defined as:

$$DBI(K) = \frac{1}{K} \sum_{i=1}^K \max\left\{ \frac{S_i + S_k}{\|z_i - z_k\|^2} \right\}, i \neq k, \quad (8)$$

where  $S_i = \frac{1}{N_i} \sum_{x_j \in C_i} \|x_j - z_i\|^2$ ,  $N_i$  denotes the number of data points in the  $i$ th cluster ( $C_i$ ).

(2) The Dunn Index ( $DI^+$ ) [28] evaluates a clustering by taking the minimum distance between-cluster as separation and the maximum distance between each pair of within-cluster points as compactness. The original index is defined as [28]:

$$Dunn(K) = \min_{1 \leq p \leq K} \left( \min_{s+1 \leq q \leq K-1} \left( \frac{dis(C_p, C_q)}{\max_{1 \leq i \leq K} dia(C_i)} \right) \right), \quad (9)$$

where  $dis(C_p, C_q)$  refers to the distance between the  $p$ th and  $q$ th clusters, is calculated as  $dis(C_p, C_q) = \min_{x_j \in C_p, x_l \in C_q} (\|x_j - x_l\|)$ ;  $dia(C_i)$  denotes the maximum distance between any pair of within-cluster points, which is measured as  $dia(C_i) = \max_{x_j, x_l \in C_i} (\|x_j - x_l\|)$ .

(3) The Calinski-Harabasz Index ( $CHI^+$ ) [29] is a ratio-type index in which compactness is measured by the distance ( $W_K$ ) between each within-cluster point to its centroid, and separation is based on the distance ( $B_K$ ) between each centroid to the global centroid ( $\bar{z}$ ), *i.e.*:

$$CHI(K) = \frac{B_K}{K-1} / \frac{W_K}{N-K}, \quad (10)$$

where  $B_K = \sum_{i=1}^K N_i \|z_i - \bar{z}\|^2$ ,  $W_K = \sum_{i=1}^K \sum_{x_j \in C_i} \|x_j - z_i\|^2$ .

(4) The Fukuyama and Sugeno Index ( $FSI^-$ ) [30] is designed to measure the discrepancy between fuzzy compactness and fuzzy separation, *i.e.*:

$$FSI(K) = \sum_{i=1}^K \sum_{j=1}^N u_{ij}^m \|x_j - z_i\|^2 - \sum_{i=1}^K \sum_{j=1}^N u_{ij}^m \|z_i - \bar{z}\|^2, \quad (11)$$

(5) The Xie and Beni Index ( $XBI^-$ ) [31] is also a ratio-type index, which measures the average within-cluster fuzzy compactness against the minimum between-cluster separation, *i.e.*:

$$XBI(K) = \frac{\sum_{i=1}^K \sum_{j=1}^N \mu_{ij}^2 \|x_j - z_i\|^2}{N \cdot \min_{i \neq k} \{ \|z_i - z_k\|^2 \}}, \quad (12)$$

(6) The Kwon Index ( $KI^-$ ) [32] aims to overcome the shortcoming of XBI that decreases monotonically when the cluster number approaches the actual cluster number of data. Here, a penalty function was introduced to the numerator of XBI, *i.e.*:

$$KI(K) = \frac{\sum_{i=1}^K \sum_{j=1}^N \mu_{ij}^2 \|x_j - z_i\|^2 + \frac{1}{K} \sum_{i=1}^K \|z_i - \bar{z}\|^2}{\min_{i \neq k} \{ \|z_i - z_k\|^2 \}}, \quad (13)$$

(7) The Tang Index (TI<sup>-</sup>) [33] also introduced a similar penalty function to the numerator of XBI, i.e.:

$$TI(K) = \frac{\sum_{i=1}^K \sum_{j=1}^N \mu_{ij}^2 \|x_j - z_i\|^2 + \frac{1}{K(K-1)} \sum_{i=1}^K \sum_{\substack{k=1 \\ k \neq i}}^K \|z_i - z_k\|^2}{\min_{i \neq k} \|z_i - z_k\|^2 + 1/K} \tag{14}$$

(8) The SC Index (SCI<sup>+</sup>) [34] measures the fuzzy compactness/separation ratio of clustering by using the difference between two functions, SC<sub>1</sub> and SC<sub>2</sub>, i.e.:

$$SCI(K) = SC_1(K) - SC_2(K), \tag{15}$$

where SC<sub>1</sub> (Equation (16)) evaluates the compactness/separation ratio by considering the grades of membership and the original data: the larger the SC<sub>1</sub>, the better the clustering:

$$SC_1(K) = \frac{(\frac{1}{K} \sum_{i=1}^K \|z_i - \bar{z}\|)}{\sum_{i=1}^K (\sum_{j=1}^N \mu_{ij}^m \|x_j - z_i\|^2 / \sum_{j=1}^N \mu_{ij})}, \tag{16}$$

while SC<sub>2</sub> (Equation (17)) measures the ratio by using the grades of membership only: the smaller the SC<sub>2</sub>, the better the clustering:

$$SC_2(K) = \frac{\sum_{i=1}^{K-1} \sum_{k=i+1}^K (\sum_{j=1}^N (\min(\mu_{ij}, \mu_{kj})^2) / n_{jk})}{(\sum_{j=1}^N \max_{1 \leq i \leq K} \mu_{ij}^2) / (\sum_{j=1}^N \max_{1 \leq i \leq K} \mu_{ij})} \tag{17}$$

where  $n_{jk} = \sum_{j=1}^N \min(\mu_{ij}, \mu_{kj})$ .

(9) The Compose Within and Between scattering Index (CWBI<sup>-</sup>) [19] assesses the average compactness and separation of fuzzy clustering by using the sum of two functions, i.e.:

$$CWBI(K) = \alpha Scat(K) + Dis(K), \tag{18}$$

where  $\alpha$  is a weighing factor which equals  $Dis(K_{max})$ , the  $Dis(K)$  with the maximum cluster number; and  $Scat(K)$  refers to the average scattering (i.e., compactness) for  $K$  clusters, which is defined as:

$$Scat(K) = \frac{\frac{1}{K} \sum_{i=1}^K \|\sigma(z_i)\|}{\|\sigma(X)\|}, \tag{19}$$

where  $\|x\| = (x^T \cdot x)^{1/2}$ ;  $\sigma(X)$  denotes the variance of data, which is defined as  $\sigma(X) = \frac{1}{N} \sum_{j=1}^N (x_j - \bar{z})^2$ ;  $\sigma(z_i)$  denotes the fuzzy variation of cluster  $i$ , which is defined as  $\sigma(z_i) = \frac{1}{N} \sum_{j=1}^N \mu_{ij}(x_j - z_i)^2$ .

The smaller the value of  $Scat(K)$ , the better the compactness of the clustering.

The distance function  $Dis(K)$  measuring the separation between clusters is defined as:

$$Dis(K) = \frac{D_{max}}{D_{min}} \sum_{i=1}^K (\sum_{k=1}^K \|z_i - z_k\|)^{-1}, \tag{20}$$

where  $D_{\max} = \max\{\|z_i - z_k\|\}$ ,  $D_{\min} = \min\{\|z_i - z_k\|\}$ ,  $i, k \in \{2, 3, \dots, K\}$ .

The smaller the value of  $Dis(K)$ , the better the separation of clusters.

(10) The WSJ Index ( $WSJI^-$ ) [13], inspired by the CWBI, also uses a linear combination of averaged fuzzy compactness and separation to measure clustering, which is defined as:

$$WSJI(K) = Scat(K) + \frac{Sep(K)}{Sep(K_{\max})} \quad (21)$$

where  $Scat(K)$  is given by Equation (19);  $Sep(K)$  denotes the between-cluster separation, which is defined as  $Sep(K) = \frac{D_{\max}^2}{D_{\min}^2} \sum_{i=1}^K (\sum_{k=1}^K \|z_i - z_k\|^2)^{-1}$ , where  $D_{\max} = \max\{\|z_i - z_k\|\}$ ,  $D_{\min} = \min\{\|z_i - z_k\|\}$ ;  $Sep(K_{\max})$  refers to the  $Sep(K)$  with the maximum cluster number.

(11) The PBMF index ( $PBMFI^+$ ) [20] estimates within-cluster compactness and large separation between clusters of fuzzy clustering, *i.e.*:

$$PBMFI(K) = \frac{\max_{i \neq k} \{\|z_i - z_k\|\} \times \sum_{j=1}^N \mu_{j1} \|x_i - z_1\|}{K \sum_{i=1}^K \sum_{j=1}^N \mu_{ij}^m \|x_j - z_i\|} \quad (22)$$

(12) The SVF index ( $SVFI^+$ ) [35] emphasizes on low within-cluster variation (*i.e.*, high compactness) and large separation between clusters, *i.e.*:

$$SVFI(K) = \frac{\sum_{i=1}^K \min_{i \neq k} \|z_i - z_k\|}{\sum_{i=1}^K \max_{x_j \in C_i} \mu_{ij}^m \|x_j - z_i\|} \quad (23)$$

(13) The WL Index ( $WLI^-$ ) [12] measures both within-cluster compactness and between-cluster separation of fuzzy clustering. Specifically, it takes both the minimum and the median distances between clusters as separation, which retains the clusters whose centroids are close to each other. The index is defined as:

$$WLI(K) = \frac{WL_n}{2WL_d} \quad (24)$$

where  $WL_n$  denotes the fuzzy compactness of clusters, which is defined as  $WL_n =$

$$\sum_{i=1}^K \left( \frac{\sum_{j=1}^N \mu_{ij}^2 \|x_j - z_i\|^2}{\sum_{j=1}^N \mu_{ij}} \right); WL_d \text{ refers to the separation between clusters, which is defined as } WL_d =$$

$\frac{1}{2} (\min_{i \neq k} \{\|z_i - z_k\|^2\} + \text{median}_{i \neq k} \{\|z_i - z_k\|^2\})$ , where  $\min_{i \neq k} \{\|z_i - z_k\|^2\}$  and  $\text{median}_{i \neq k} \{\|z_i - z_k\|^2\}$  denote, respectively, the minimum distance and median distance between any pair of clusters.

#### 4. Experiments and Results

In this section, the performance of the 16 CVIs introduced in Section 3 was evaluated using five types of multispectral, and four types of hyperspectral, remote sensing datasets (detailed below). For image clustering, the FCM and K-means algorithms were utilized here. The operational parameters in FCM were designated in line with previous studies [13]: threshold of iteration termination  $\varepsilon = e - 5$ , weighting exponent  $m = 2$ , and the maximum iteration number  $Max\_iter = 500$ ; while the operational parameters in K-means as: the pixel change threshold = 0%, and the maximum iteration number  $Max\_iter = 500$ . For each of the images, the two algorithms were implemented with cluster number

$K = 2, 3, \dots, 10$ , respectively. To overcome the shortcoming of the two algorithms that often trap on local optima, depending on the initial solutions [36], each implementation of the clustering was repeated five times and the best clustering result (with the minimum value of  $J_m$  (Equation (1)) or  $M$  (Equation (4)) was retained for CVIs evaluation.

4.1. Datasets

The five multispectral data sets include QuickBird [37], Landsat TM, Landsat ETM+, GaoFen-1 [38], and FLC1 [39]. Their true/false color maps, the corresponding ground reference maps and the spectral curves of land use/cover classes were shown in Figure 1. The four hyperspectral datasets include Hyperion [40], HYDICE [41], ROSIS [42] and AVIRIS [43]. Their false color maps, ground reference maps and spectral curves of land cover/use classes were presented in Figure 2. The basic information on the remote sensing datasets employed in our experiments was detailed in Table 1.

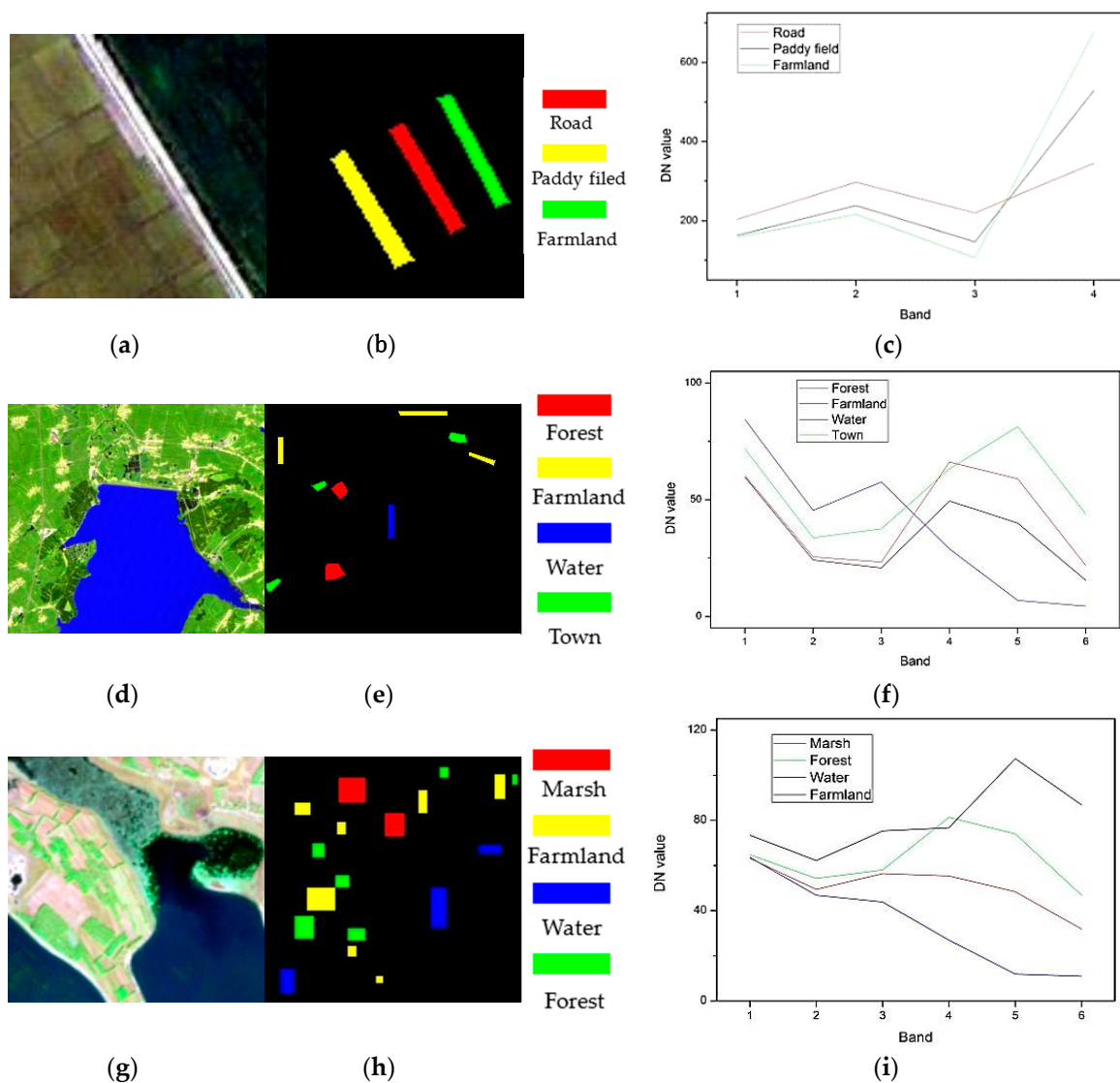
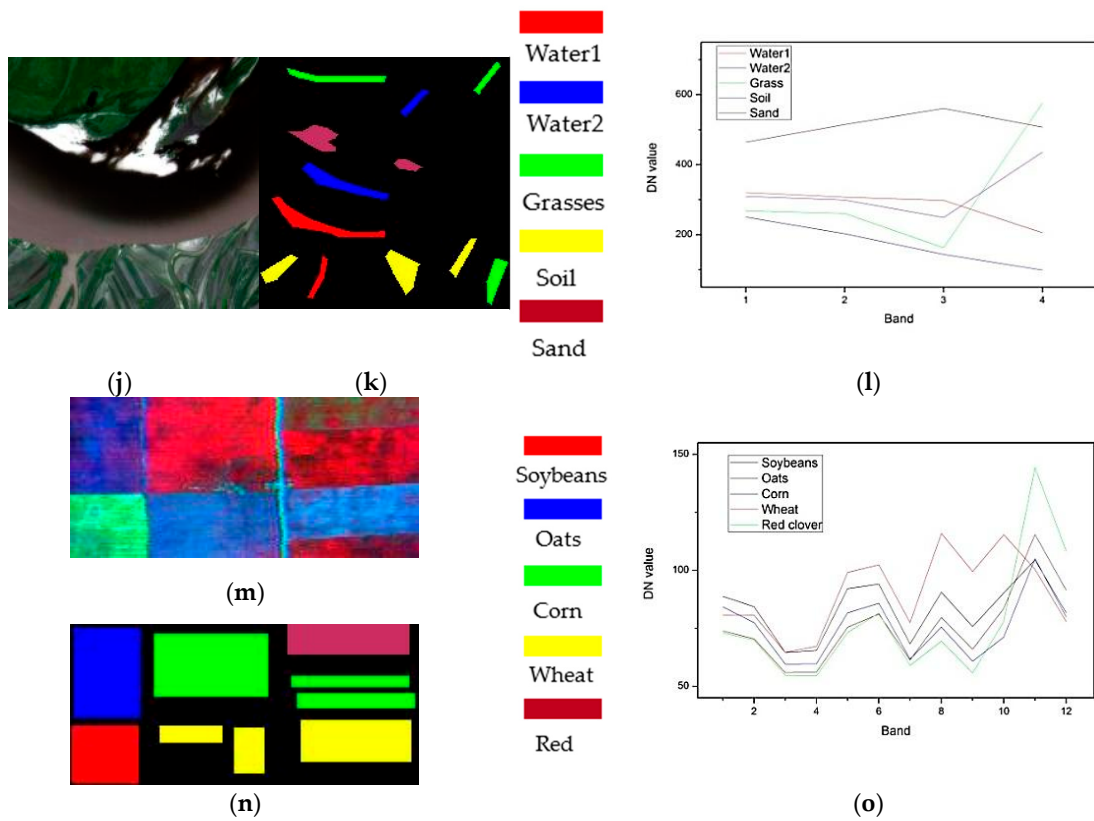
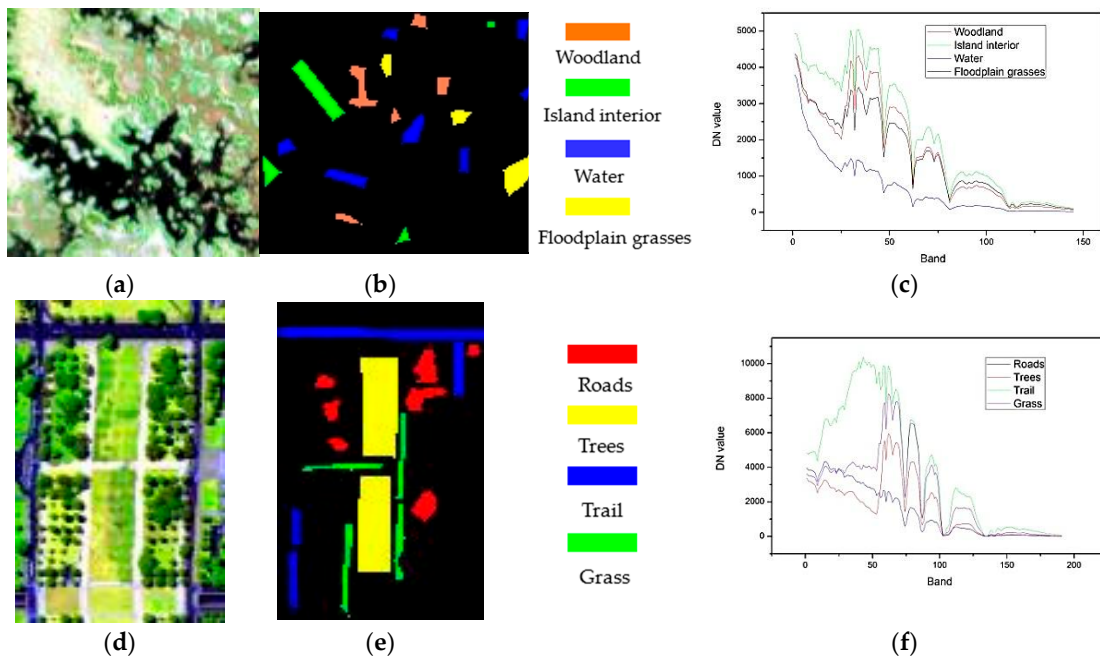


Figure 1. Cont.



**Figure 1.** The multispectral images. (a–c) the true/false color map, the ground reference map and the corresponding spectral curves of ground truth classes of QuickBird datasets; (d–f) the corresponding maps of Landsat TM datasets; (g–i) the corresponding maps of Landsat ETM+ datasets; (j–l) the corresponding maps of GaoFen-1 datasets; (m–o) the corresponding maps of FLC1 datasets. (a) True color map; (b) false color map (7, 5, 3); (c) false color map (7, 5, 3); (d) true color map; and (e) false color map (bands 12, 9, and 1).



**Figure 2.** Cont.

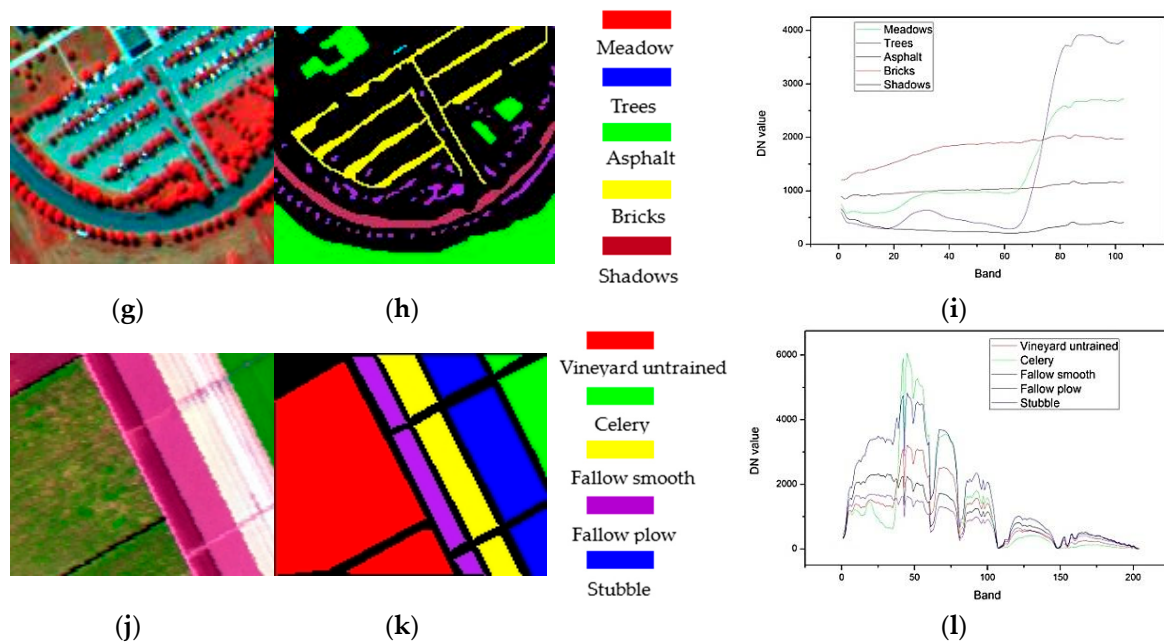


**Figure 2.** The hyperspectral images. (a–c) the false color (FC) map, the corresponding ground reference map and the corresponding spectral curves of ground truth classes of Hyperion data sets; (d–f) the corresponding maps of HYDICE datasets; (g–i) the corresponding maps of ROSIS datasets; (j–l) the corresponding maps of AVIRIS datasets. (a) FC map (bands 93, 60, 10); (b) FC map (bands 120, 90, 10); (c) FC map (bands 90, 60, 10); and (d) FC map (bands 111, 90, 12).

**Table 1.** Basic information of the remote sensing data sets.

D	S	Y	L	R	B	W	S	GT
QuickBird	Multi-spectral camera	2005	Yalvhe farm, China	2.4	4	0.45–0.90	100 × 100	Road, paddy field, and farmland
Landsat TM	Thematic mapper	2005	JingYuetan reservoir, China	30	6	0.45–2.35	296 × 295	Forest, farmland, water, and town
Landsat ETM+	Enhanced thematic mapper	2001	Zhalong reserve, China	30	6	0.45–2.35	150 × 139	Marsh, forest, water, and farmland
Gaofen-1	Wide filed imager	2015	Sanjiang Plain, China	16	4	0.45–0.89	200 × 200	Water1, water2, grass, soil, and sand
FLC1	M7 scanner	1966	Tippecanoe County, US	30	12	0.40–1.00	84 × 183	Soybeans, oats, corn, wheat and red clover
Hyperion	Hyperion	2001	Okavango Delta, Botswana	30	145	0.40–2.50	126 × 146	Woodland, island interior, water and floodplain grasses
HYDICE	HYDICE	1995	Washington DC, US	2	191	0.40–2.40	126 × 82	Roads, trees, trail and grass
ROSIS	ROSIS	2001	University of Pavia, Italy	1.3	103	0.43–0.86	125 × 148	Meadows, trees, asphalt, bricks and shadows
AVIRIS	AVIRIS	1998	Salinas Valley, USA	3.7	204	0.41–2.45	117 × 143	Vineyard untrained, celery, fallow smooth, fallow plow and stubble

Note: D, datasets; S, sensor; Y, year; L, location; R, resolution (m); B, number of bands; W, spectral wavelength ( $\mu\text{m}$ ); S, size of image (pixel by pixels); GT, ground truth classes.

#### 4.2. Results

The nine types of images were clustered by FCM and K-means algorithms respectively, and each clustering result was evaluated using the corresponding ground-truth data (Figures 1 and 2). Table 2 shows the classification accuracies of the images achieved by the two algorithms. Similarly, both FCM and K-means generated good classification results, with the overall accuracy greater than 90%

for seven images. However, considering the length limitation of the paper, the clustering results by K-means and the corresponding cluster validity result for each image were not presented in as much detail as those by FCM, but were summarized at the end of the results.

**Table 2.** Classification accuracies of the remote sensing images acquired by FCM and K-means algorithms.

Datasets	K#	Overall Accuracies (%)		Kappa Coefficient	
		FCM	K-Means	FCM	K-Means
QuickBird	3	96.06	96.10	0.9354	0.9361
Landsat TM	4	95.78	95.27	0.9433	0.9363
Landsat ETM+	4	94.41	96.30	0.9253	0.9565
Gaofen-1	5	98.34	98.79	0.9791	0.9848
FLC1	5	83.10	84.48	0.7847	0.8016
Hyperion	4	87.09	86.79	0.8260	0.8219
HYDICE	4	94.88	96.00	0.9238	0.9403
ROSIS	5	93.85	93.25	0.9129	0.9044
AVIRIS	5	99.63	99.63	0.9946	0.9946

Tables 3–11 illustrated the variations of the 16 CVIs with the number of clusters ranging from two to 10 by FCM for each image. The optimal cluster numbers of each image are indicated by the CVIs, shown in bold font. The clustering results of multispectral and hyperspectral datasets by FCM, respectively, are illustrated in Figures 3 and 4. Note that only four clustering results for each image are presented, including the optimal one (underlined), one or two close to the optimal, and those indicated by many CVIs (usually larger than 4) (bold). For example, Figure 3e–h illustrates the clustering results of Landsat TM image, in which the optimal clustering (Figure 3g) is underlined, the two near-optimal clustering results (Figure 3f,h) and the obviously-incorrect clustering indicated by many CVIs (Figure 3e) are also presented.

**Table 3.** Variations of the 16 CVIs with cluster numbers ranging from 2 to 10 for the QuickBird image.

CVIs	Cluster Number								
	2	3 *	4	5	6	7	8	9	10
PC <sup>+</sup>	0.754	<b>0.800</b>	0.728	0.699	0.658	0.623	0.626	0.593	0.579
PE <sup>-</sup>	0.565	<b>0.532</b>	0.749	0.866	1.008	1.134	1.150	1.272	1.341
MPC <sup>+</sup>	0.509	<b>0.700</b>	0.637	0.624	0.590	0.560	0.572	0.542	0.533
DBI <sup>-</sup>	0.822	<b>0.559</b>	0.692	0.750	0.779	0.845	0.802	0.882	0.915
DI <sup>+</sup> (e-3)	2.486	<b>3.591</b>	2.539	2.539	2.614	2.614	3.439	3.439	3.439
CHI <sup>+</sup> (e4)	1.142	2.041	2.026	2.030	1.908	1.779	<b>2.116</b>	1.998	1.971
FSI <sup>-</sup> (e7)	-0.535	-6.644	-7.247	-7.331	-7.093	-6.902	<b>-7.440</b>	-7.260	-7.092
XBI <sup>-</sup>	0.160	<b>0.103</b>	0.218	0.236	0.231	0.287	0.237	0.325	0.277
KI <sup>-</sup> (e3)	1.601	<b>1.027</b>	2.184	2.370	2.312	2.883	2.382	3.266	2.790
TI <sup>-</sup> (e3)	1.601	<b>1.029</b>	2.189	2.376	2.320	2.894	2.395	3.284	2.808
SCI <sup>+</sup>	0.477	2.477	2.516	2.752	2.837	2.554	<b>3.546</b>	3.456	3.349
CWBI <sup>-</sup> (e-2)	4.076	<b>2.826</b>	4.284	4.964	5.399	6.902	6.592	8.628	8.499
WSJI <sup>-</sup>	0.365	<b>0.171</b>	0.256	0.339	0.399	0.648	0.618	1.060	1.023
PBMFI <sup>+</sup> (e3)	1.588	<b>3.214</b>	0.635	0.336	0.068	0.060	0.022	0.034	0.013
SVFI <sup>+</sup>	1.422	2.415	2.621	2.910	3.063	3.252	3.517	3.699	<b>3.885</b>
WLI <sup>-</sup>	0.339	<b>0.252</b>	0.325	0.418	0.426	0.453	0.346	0.374	0.388

Note: \* denotes the actual cluster number of the image; figures in bold face denote the optimal cluster numbers of the image identified by the CVIs; the data in the brackets of the first column is a multiplying factor (e.g., e-3 followed DI<sup>+</sup>) of the corresponding line.

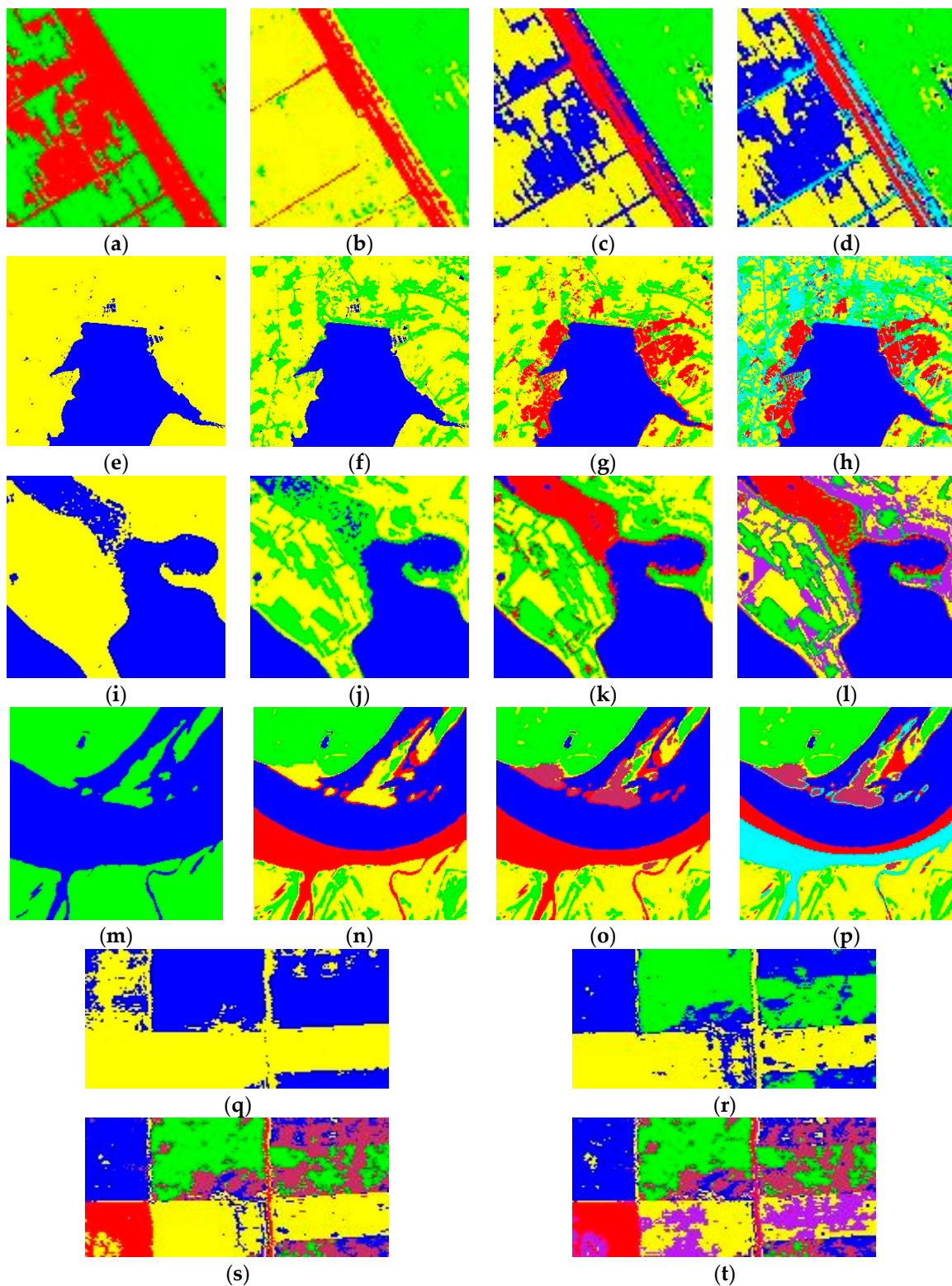


**Figure 3.** Clustering results of the multispectral images (each color represents a cluster). (a) QuickBird,  $K = 2$ ; (b) QuickBird,  $K = 3$ ; (c) QuickBird,  $K = 4$ ; (d) QuickBird,  $K = 5$ ; (e) Landsat TM,  $K = 2$ ; (f) Landsat TM,  $K = 3$ ; (g) Landsat TM,  $K = 4$ ; (h) Landsat TM,  $K = 5$ ; (i) Landsat ETM+,  $K = 2$ ; (j) Landsat ETM+,  $K = 3$ ; (k) Landsat ETM+,  $K = 4$ ; (l) Landsat ETM+,  $K = 5$ ; (m) GaoFen-1,  $K = 2$ ; (n) GaoFen-1,  $K = 4$ ; (o) GaoFen-1,  $K = 5$ ; (p) GaoFen-1,  $K = 6$ ; (q) FLC1,  $K = 2$ ; (r) FLC1,  $K = 3$ ; (s) FLC1,  $K = 5$ ; and (t) FLC1,  $K = 6$ .

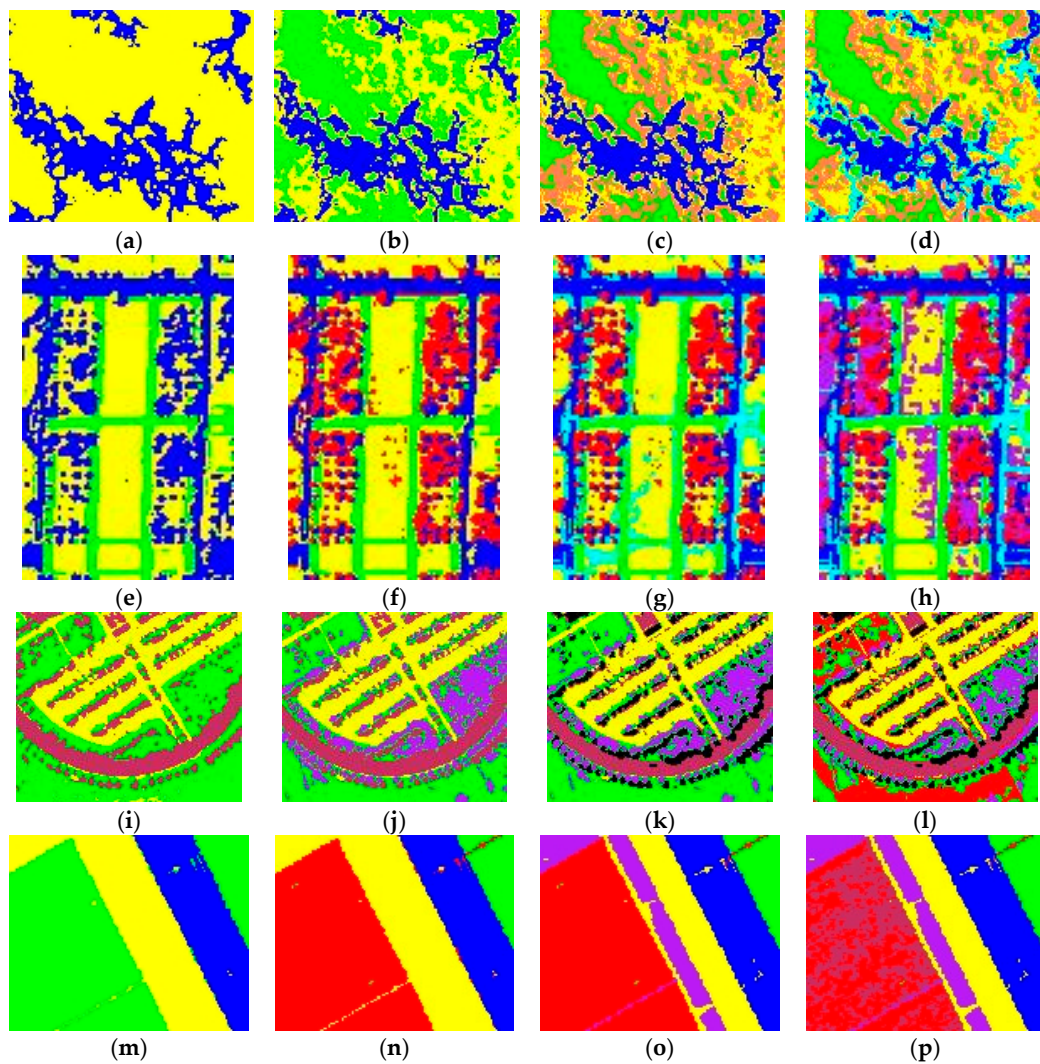


**Figure 4.** Clustering results of the hyperspectral images by FCM (each color represents a cluster). (a) **Hyperion**,  $K = 2$ ; (b) **Hyperion**,  $K = 3$ ; (c) **Hyperion**,  $K = 4$ ; (d) **Hyperion**,  $K = 5$ ; (e) **HYDICE**,  $K = 3$ ; (f) **HYDICE**,  $K = 4$ ; (g) **HYDICE**,  $K = 5$ ; (h) **HYDICE**,  $K = 6$ ; (i) **ROSIS**,  $K = 3$ ; (j) **ROSIS**,  $K = 4$ ; (k) **ROSIS**,  $K = 5$ ; (l) **ROSIS**,  $K = 6$ ; (m) **AVIRIS**,  $K = 3$ ; (n) **AVIRIS**,  $K = 4$ ; (o) **AVIRIS**,  $K = 5$ ; and (p) **AVIRIS**,  $K = 6$ .

**Table 4.** Variations of the 16 CVIs with cluster numbers ranging from 2 to 10 for the Landsat TM image.

CVIs	Cluster Number								
	2	3	4 *	5	6	7	8	9	10
PC <sup>+</sup>	0.922	0.796	0.794	0.689	0.657	0.610	0.587	0.571	0.472
PE <sup>-</sup>	0.204	0.521	0.587	0.856	0.998	1.168	1.281	1.354	1.593
MPC <sup>+</sup>	0.844	0.695	0.726	0.612	0.589	0.545	0.528	0.517	0.413
DBI <sup>-</sup>	0.282	0.764	0.601	0.999	0.913	1.055	1.064	1.185	1.522
DI <sup>+</sup> (e-3)	8.00	7.548	7.783	8.042	8.498	8.893	8.893	8.893	8.893
CHI <sup>+</sup> (e5)	2.883	2.608	3.261	2.914	2.831	2.568	2.393	2.348	2.053
FSI <sup>-</sup> (e7)	-6.762	-7.850	-8.743	-8.423	-8.342	-8.132	-8.027	-7.945	-5.888
XBI <sup>-</sup>	0.044	0.177	0.092	0.599	0.450	0.626	0.564	0.661	2.025
KI <sup>-</sup> (e4)	0.334	1.335	0.693	4.523	3.402	4.731	4.259	4.996	15.300
TI <sup>-</sup> (e4)	0.334	1.335	0.693	4.515	3.397	4.721	4.251	4.985	15.188
SCI <sup>+</sup>	3.463	3.319	3.876	3.609	3.407	2.916	3.204	2.362	3.439
CWBI <sup>-</sup> (e-2)	0.151	0.142	0.114	0.291	0.299	0.403	0.425	0.457	0.762
WSJI <sup>-</sup>	0.167	0.094	0.057	0.154	0.159	0.274	0.307	0.372	1.015
PBMFI <sup>+</sup> (e3)	1.014	0.296	0.018	0.013	0.006	0.006	0.001	0.001	0.001
SVFI <sup>+</sup>	1.922	2.287	2.982	3.367	3.816	4.106	4.349	4.224	3.137
WLI <sup>-</sup>	0.079	0.131	0.172	0.247	0.327	0.361	0.463	0.395	0.293

Note: \* denotes the actual cluster number of the image.

**Table 5.** Variations of the 16 CVIs with cluster numbers ranging from 2 to 10 for the ETM+ image.

CVIs	Cluster Number								
	2	3	4 *	5	6	7	8	9	10
PC <sup>+</sup>	0.404	<b>0.812</b>	0.760	0.725	0.703	0.663	0.628	0.617	0.593
PE <sup>-</sup>	<b>0.284</b>	0.503	0.673	0.802	0.877	1.012	1.144	1.204	1.300
MPC <sup>+</sup>	<b>0.775</b>	0.717	0.680	0.656	0.644	0.607	0.575	0.569	0.548
DBI <sup>-</sup>	<b>0.404</b>	0.603	0.674	0.731	0.745	0.861	0.952	0.937	1.055
DI <sup>+</sup> (e-3)	5.803	7.595	8.256	<b>8.889</b>	8.889	0.104	0.107	0.107	0.114
CHI <sup>+</sup> (e5)	0.818	0.909	<b>0.929</b>	0.929	0.896	0.893	0.847	0.847	0.822
FSI <sup>-</sup> (e8)	-0.409	<b>-0.483</b>	-0.477	-0.461	-0.461	-0.439	-0.426	-0.422	-0.413
XBI <sup>-</sup>	<b>0.047</b>	0.090	0.117	0.169	0.183	0.202	0.234	0.216	0.293
KI <sup>-</sup> (e4)	<b>0.100</b>	0.188	0.244	0.352	0.382	0.421	0.489	0.452	0.613
TI <sup>-</sup> (e4)	<b>0.099</b>	0.189	0.244	0.353	0.383	0.422	0.490	0.454	0.615
SCI <sup>+</sup>	2.463	3.259	3.388	3.723	4.715	<b>5.137</b>	4.922	4.779	4.884
CWBI <sup>-</sup>	<b>0.054</b>	0.059	0.076	0.104	0.112	0.133	0.164	0.174	0.226
WSJI <sup>-</sup>	0.162	0.351	<b>0.126</b>	0.214	0.248	0.348	0.515	0.601	1.012
PBMFI <sup>+</sup> (e3)	<b>1.058</b>	0.156	0.085	0.088	0.004	0.005	0.002	0.014	0.003
SVFI <sup>+</sup>	2.173	2.413	3.027	0.760	3.155	3.339	3.521	3.607	<b>3.648</b>
WLI <sup>-</sup>	<b>0.093</b>	0.174	0.307	0.265	0.244	0.229	0.259	0.208	0.279

Note: \* denotes the actual cluster number of the image.

**Table 6.** Variations of the 16 CVIs with cluster numbers ranging from 2 to 10 for the GaoFen-1 image.

CVIs	Cluster Number								
	2	3	4	5 *	6	7	8	9	10
PC <sup>+</sup>	<b>0.850</b>	0.751	0.764	0.779	0.735	0.710	0.688	0.669	0.645
PE <sup>-</sup>	<b>0.374</b>	0.643	0.663	0.658	1.183	0.900	0.978	1.056	1.140
MPC <sup>+</sup>	0.700	0.627	0.620	<b>0.724</b>	0.682	0.662	0.643	0.628	0.606
DBI <sup>-</sup>	0.587	0.832	0.767	<b>0.536</b>	0.701	0.740	0.789	0.803	0.896
DI <sup>+</sup> (e-3)	<b>4.715</b>	1.478	1.470	2.298	2.348	2.688	3.028	2.860	2.965
CHI <sup>+</sup> (e5)	0.764	0.656	0.681	<b>1.314</b>	1.185	1.262	1.270	1.257	1.197
FSI <sup>-</sup> (e9)	-0.662	-1.038	-1.253	<b>-1.603</b>	-1.571	-1.539	-1.519	-1.490	-1.462
XBI <sup>-</sup>	0.100	0.135	0.136	<b>0.077</b>	0.198	0.158	0.140	0.154	0.285
KI <sup>-</sup> (e4)	0.399	0.541	0.546	<b>0.309</b>	0.791	0.634	0.560	0.617	1.141
TI <sup>-</sup> (e4)	0.399	0.541	0.546	<b>0.309</b>	0.792	0.635	0.561	0.618	1.141
SCI <sup>+</sup>	1.031	1.156	1.364	<b>4.658</b>	3.899	4.468	4.470	4.333	3.992
CWBI <sup>-</sup> (e-3)	0.147	<b>0.137</b>	0.144	0.139	0.240	0.264	0.268	0.311	0.445
WSJI <sup>-</sup>	0.226	0.934	0.128	<b>0.114</b>	0.282	0.348	0.362	0.487	1.015
PBMFI <sup>+</sup> (e4)	<b>1.049</b>	0.243	0.075	0.053	0.063	0.019	0.011	0.040	0.056
SVFI <sup>+</sup>	2.315	2.610	3.027	3.707	3.739	<b>4.193</b>	4.009	4.245	4.165
WLI <sup>-</sup>	0.201	0.342	0.307	<b>0.154</b>	0.174	0.202	0.196	0.208	0.226

Note: \* denotes the actual cluster number of the image.

**Table 7.** Variations of the 16 CVIs with cluster numbers ranging from 2 to 10 for the FLC1 image.

CVIs	Cluster Number								
	2	3	4	5 *	6	7	8	9	10
PC <sup>+</sup>	<b>0.760</b>	0.680	0.584	0.602	0.555	0.497	0.451	0.429	0.398
PE <sup>-</sup>	<b>0.549</b>	0.834	1.139	1.160	1.343	1.556	1.724	1.831	1.974
MPC <sup>+</sup>	0.519	<b>0.520</b>	0.446	0.503	0.466	0.414	0.372	0.358	0.331
DBI <sup>-</sup>	<b>0.887</b>	0.909	1.052	0.896	0.937	1.008	1.432	1.410	1.475
DI <sup>+</sup> (e-2)	0.806	1.330	1.048	<b>1.613</b>	1.365	1.495	1.259	1.259	1.542
CHI <sup>+</sup> (e4)	1.274	1.537	1.273	<b>1.616</b>	1.521	1.354	1.249	1.194	1.105
FSI <sup>-</sup> (e6)	-0.666	-5.029	-5.479	<b>-8.809</b>	-8.573	-7.979	-7.511	-7.200	-6.794
XBI <sup>-</sup>	0.206	<b>0.186</b>	0.380	0.224	0.268	0.334	0.636	0.616	0.576
KI <sup>-</sup> (e4)	0.299	<b>0.270</b>	0.552	0.325	0.390	0.485	0.924	0.896	0.837
TI <sup>-</sup> (e4)	0.299	<b>0.270</b>	0.552	0.325	0.390	0.485	0.924	0.896	0.838
SCI <sup>+</sup>	0.307	0.624	0.383	0.913	<b>1.089</b>	0.672	0.639	0.815	0.681
CWBI <sup>-</sup>	0.126	<b>0.098</b>	0.123	0.109	0.128	0.154	0.221	0.230	0.238
WSJI <sup>-</sup>	0.410	0.598	0.294	<b>0.241</b>	0.305	0.425	0.877	0.968	1.049
PBMFI <sup>+</sup>	<b>186.178</b>	84.915	27.891	5.076	16.638	5.969	5.374	2.140	0.932
SVFI <sup>+</sup>	1.185	1.874	2.389	3.040	3.424	3.680	3.439	3.679	<b>3.803</b>
WLI <sup>-</sup>	<b>0.415</b>	0.535	0.708	0.523	0.584	0.709	7.591	0.727	0.777

Note: \* denotes the actual cluster number of the image.

**Table 8.** Variations of the 16 CVIs with cluster numbers ranging from 2 to 10 for the Hyperion image.

CVIs	Cluster Number								
	2	3	4 *	5	6	7	8	9	10
PC <sup>+</sup>	<b>0.867</b>	0.759	0.682	0.658	0.596	0.568	0.530	0.494	0.476
PE <sup>-</sup>	<b>0.337</b>	0.626	0.869	0.973	1.176	1.293	1.435	1.577	1.666
MPC <sup>+</sup>	<b>0.735</b>	0.638	0.576	0.573	0.515	0.496	0.463	0.430	0.417
DBI <sup>-</sup>	<b>0.472</b>	0.651	0.732	0.726	0.853	0.856	0.946	1.060	1.032
DI <sup>+</sup> (e-2)	2.169	2.979	2.837	2.900	3.489	3.332	3.518	2.971	<b>3.916</b>
CHI <sup>+</sup> (e4)	4.690	5.329	5.328	<b>5.779</b>	5.485	5.383	5.158	4.925	4.846
FSI <sup>-</sup> (e11)	-4.610	-6.600	-6.902	-7.003	<b>-6.808</b>	-6.619	-6.414	-6.209	-6.039
XBI <sup>-</sup>	<b>0.061</b>	0.139	0.157	0.149	0.217	0.193	0.228	0.275	0.239
KI <sup>-</sup> (e3)	<b>1.131</b>	2.552	2.888	2.750	3.995	3.560	4.201	5.064	4.400
TI <sup>-</sup> (e3)	<b>1.131</b>	2.555	2.892	2.755	4.004	3.569	4.213	5.080	4.416
SCI <sup>+</sup>	2.241	3.109	3.161	4.201	4.012	4.586	4.574	4.469	<b>4.605</b>
CWBI <sup>-</sup> (e-3)	<b>0.440</b>	0.485	0.597	0.651	0.900	0.929	1.118	1.347	1.333
WSJI <sup>-</sup>	0.244	0.681	<b>0.207</b>	0.244	0.446	0.491	0.706	1.019	1.020
PBMFI <sup>+</sup> (e6)	4.131	<b>6.247</b>	1.732	0.319	0.528	0.325	0.184	0.009	0.005
SVFI <sup>+</sup>	2.204	2.459	2.867	3.124	3.307	3.536	3.697	3.764	<b>3.885</b>
WLI <sup>-</sup>	1.222	<b>0.185</b>	0.241	0.231	0.242	0.244	0.254	0.281	0.307

Note: \* denotes the actual cluster number of the image.

**Table 9.** Variations of the 16 CVIs with cluster numbers ranging from 2 to 10 for the HYDICE image.

CVIs	Cluster Number								
	2	3	4 *	5	6	7	8	9	10
PC <sup>+</sup>	<b>0.752</b>	0.729	0.669	0.621	0.587	0.554	0.541	0.511	0.502
PE <sup>-</sup>	<b>0.573</b>	0.717	0.922	1.106	1.246	1.382	1.471	1.598	1.656
MPC <sup>+</sup>	0.504	<b>0.594</b>	0.558	0.526	0.505	0.479	0.475	0.450	0.447
DBI <sup>-</sup>	0.888	<b>0.669</b>	0.747	0.824	0.828	0.899	0.827	0.888	0.888
DI <sup>+</sup> (e-2)	1.194	1.070	1.165	1.236	1.081	1.190	<b>1.897</b>	1.098	1.089
CHI <sup>+</sup> (e4)	1.057	1.494	1.473	<b>1.618</b>	1.606	1.508	1.634	1.587	1.594
FSI <sup>-</sup> (e12)	0.004	-1.258	-1.511	-1.592	<b>-1.627</b>	-1.603	-1.608	-1.579	-1.567
XBI <sup>-</sup>	0.196	<b>0.105</b>	0.149	0.168	0.231	0.258	0.223	0.315	0.260
KI <sup>-</sup> (e3)	2.025	<b>1.084</b>	1.545	1.733	2.393	2.671	2.306	3.258	2.694
TI <sup>-</sup> (e3)	2.026	<b>1.085</b>	1.547	1.737	2.398	2.678	2.313	3.268	2.704
SCI <sup>+</sup>	0.391	1.878	1.906	1.997	<b>2.151</b>	1.733	1.911	1.691	1.901
CWBI <sup>-</sup> (e-4)	2.538	<b>1.761</b>	2.017	2.395	3.082	3.508	3.585	4.598	4.398
WSJI <sup>-</sup>	0.422	1.082	<b>0.229</b>	0.299	0.482	0.621	0.671	1.111	1.034
PBMFI <sup>+</sup> (e6)	27.978	<b>28.242</b>	7.311	1.490	2.274	1.228	0.250	0.655	0.118
SVFI <sup>+</sup>	1.560	2.490	2.928	3.298	3.566	3.689	4.202	<b>4.352</b>	4.349
WLI <sup>-</sup>	0.390	<b>0.263</b>	0.288	0.323	0.388	0.406	0.475	0.474	0.387

Note: \* denotes the actual cluster number of the image.

**Table 10.** Variations of the 16 CVIs with cluster numbers ranging from 2 to 10 for the ROSIS image.

CVIs	Cluster Number								
	2	3	4	5 *	6	7	8	9	10
PC <sup>+</sup>	<b>0.703</b>	0.664	0.615	0.594	0.548	0.504	0.477	0.461	0.443
PE <sup>-</sup>	<b>0.661</b>	0.878	1.076	1.204	1.381	1.541	1.672	1.775	1.874
MPC <sup>+</sup>	0.406	<b>0.495</b>	0.486	0.492	0.457	0.421	0.403	0.393	0.381
DBI <sup>-</sup>	1.305	<b>0.796</b>	0.894	0.876	1.001	1.464	1.405	1.371	1.349
DI <sup>+</sup> (e-2)	0.580	0.656	<b>0.711</b>	0.678	0.676	0.606	0.628	0.562	0.562
CHI <sup>+</sup> (e4)	0.834	<b>1.323</b>	1.217	1.109	1.000	0.980	0.905	0.844	0.777
FSI <sup>-</sup> (e11)	2.514	-1.127	-1.939	-2.526	<b>-2.678</b>	-2.627	-2.636	-2.671	-2.637
XBI <sup>-</sup>	0.427	<b>0.158</b>	0.273	0.213	0.481	0.715	0.666	0.623	0.591
KI <sup>-</sup> (e4)	0.790	<b>0.293</b>	0.506	0.394	0.890	1.324	1.233	1.154	1.094
TI <sup>-</sup> (e4)	0.790	<b>0.293</b>	0.506	0.394	0.891	1.325	1.234	1.155	1.095
SCI <sup>+</sup>	-0.011	0.316	0.287	0.390	0.206	0.333	0.179	0.147	<b>0.591</b>
CWBI <sup>-</sup> (e-3)	0.731	<b>0.424</b>	0.493	0.451	0.700	0.872	0.946	1.009	1.082
WSJI <sup>-</sup>	0.502	0.743	0.261	<b>0.224</b>	0.432	0.660	0.789	0.913	1.058
PBMFI <sup>+</sup> (e6)	<b>2.883</b>	1.809	0.068	0.014	0.010	0.015	0.007	0.003	0.002
SVFI <sup>+</sup>	0.569	1.720	2.187	2.958	3.290	3.163	3.658	4.011	<b>4.288</b>
WLI <sup>-</sup>	0.859	<b>0.453</b>	0.624	0.665	0.872	0.678	0.848	0.857	0.848

Note: \* denotes the actual cluster number of the image.

**Table 11.** Variations of the 16 CVIs with cluster numbers ranging from 2 to 10 for the AVIRIS image.

CVIs	Cluster Number								
	2	3	4	5 *	6	7	8	9	10
PC <sup>+</sup>	0.843	0.838	<b>0.856</b>	0.732	0.763	0.700	0.681	0.661	0.631
PE <sup>-</sup>	<b>0.395</b>	0.451	0.451	0.760	0.691	0.889	0.945	1.014	1.135
MPC <sup>+</sup>	0.686	0.757	<b>0.808</b>	0.665	0.715	0.650	0.636	0.619	0.590
DBI <sup>-</sup>	0.690	0.557	<b>0.383</b>	0.689	0.617	0.802	0.864	0.949	0.962
DI <sup>+</sup> (e-2)	0.615	1.524	<b>1.567</b>	0.871	1.198	1.236	1.523	1.297	1.312
CHI <sup>+</sup> (e4)	2.105	2.991	5.686	4.681	6.460	5.642	<b>6.716</b>	6.230	5.556
FSI <sup>-</sup> (e11)	-1.098	-4.465	-6.317	-5.999	<b>-6.803</b>	-6.631	-6.331	-6.151	-6.004
XBI <sup>-</sup>	0.117	0.125	<b>0.065</b>	0.797	0.562	0.948	0.696	0.643	0.829
KI <sup>-</sup> (e4)	0.195	0.210	<b>0.109</b>	1.335	0.943	1.589	1.168	1.080	1.394
TI <sup>-</sup> (e4)	0.195	0.210	<b>0.109</b>	1.338	0.946	1.595	1.173	1.086	1.401
SCI <sup>+</sup>	1.113	1.958	4.715	3.844	5.684	4.813	5.351	5.869	<b>6.006</b>
CWBI <sup>-</sup> (e-3)	0.982	0.545	<b>0.407</b>	1.257	1.367	2.082	1.938	1.997	2.376
WSJI <sup>-</sup>	0.360	0.665	<b>0.079</b>	0.276	0.335	0.742	0.676	0.721	1.016
PBMFI <sup>+</sup> (e5)	<b>21.751</b>	14.564	0.855	4.139	0.950	1.279	1.925	0.910	1.002
SVFI <sup>+</sup>	1.942	2.653	3.414	3.544	3.620	<b>4.129</b>	3.422	3.220	3.007
WLI <sup>-</sup>	0.235	0.213	<b>0.127</b>	0.173	0.149	0.200	0.158	0.152	0.135

Note: \* denotes the actual cluster number of the image.

Figure 3a–d shows the clustering results of the simple QuickBird image with the cluster number  $K = 2, 3, 4, 5$ . The three ground truth classes (road, paddy field, and farmland) of the image were well identified with cluster number  $K = 3$  (Figure 3b). As listed in Table 3, the majority of CVIs correctly indicated the actual cluster number of this simple image (except CHI, FSI, SCI, and SVFI).

Figure 3e–h illustrates the clustering results of the Landsat TM image with the cluster number  $K = 2, 3, 4, 5$ . Among them, the clustering with  $K = 4$  succeeded in separating the four ground truth classes of the image (forest, farmland, water, and town) (Figure 3g). The clustering with  $K = 2$  was obviously incorrect since three ground truth classes, *i.e.*, forest, farmland, and town were merged into one class (Figure 3e). Unfortunately, as shown in Table 4 most indices (DBI, PC, PE, MPC, XBI, KI, TI, PBMFI, and WLI) underestimated the real situation, which preferred two as the cluster number of the image; whereas a clear overestimation was given by DI and SVFI; only five CVIs including CHI, FSI, SCI, CWBI, and WSJI provided the actual cluster number of the image.

Figure 3i–l portrays the clustering results of the Landsat ETM+ image with the cluster number  $K = 2, 3, 4, 5$ , respectively. The four ground truth classes of the image (marsh, forest, water, and farmland) were well separated with cluster number  $K = 4$  (Figure 3k). However, similar to the Landsat TM experiment, most indices (PE, MPC, XBI, KI, TI, CWBI, PBMFI, and WLI) recommended two clusters as the optimal partitioning of the image (Table 5). CHI and WSJI were the only two indices that correctly indicated the cluster number of the image.

Figure 3m–p presents the clustering results of the GaoFen-1 image with the cluster number  $K = 2, 4, 5, 6$ . The five ground truth classes of the image, namely water1 (light colored), water2 (dark colored), grass, soil, and sand, were well distinguished with cluster number  $K = 5$  (Figure 3o). This was correctly indicated by most CVIs including DBI, CHI, MPC, FSI, XBI, KI, TI, SCI, WSJI, and WLI (Table 6). For the rest of the CVIs that erroneously indicated the cluster number, most of them (DI, PC, PE, and PBMFI) suggested two.

Figure 3q–t demonstrates the clustering results of the FLC1 image with the cluster number  $K = 2, 3, 5, 6$ . The five ground truth classes of the image (soybeans, oats, corn, wheat, and red clover) were fairly well identified with cluster number  $K = 5$  (Figure 3s). For the cases of clustering with  $K = 2$  and  $K = 3$ , obvious misclassifications were observed, with some separated classes being merged into one class (Figure 3q,r). As shown in Table 7, there were four CVIs (DI, CHI, FSI, and WSJI) that provided the actual cluster number ( $K = 5$ ) for the image. But five CVIs (DBI, PC, PE, PBMFI, and WLI) and five others (MPC, XBI, KI, TI, and CWBI) erroneously supported the clustering with cluster number  $K = 2$  and  $K = 3$ , respectively.

Figure 4a–d depicts the clustering results of Hyperion data with the cluster number  $K = 2, 3, 4, 5$ . The four ground truth classes (woodland, island interior, water, and floodplain grasses) were well classified with cluster number  $K = 4$  (Figure 4c). Clustering results with other cluster numbers were

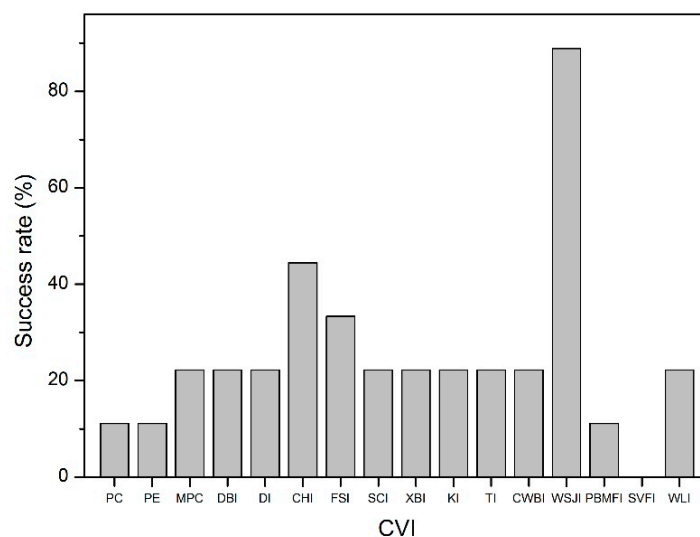
obviously not satisfactory. For example, in the case of clustering with  $K = 2$ , three (without water) of the four classes were wrongly merged into one class (Figure 4a). This was chosen by half the total CVIs, namely DBI, PC, PE, MPC, XBI, KI, TI, and CWBI (Table 8). In fact, all of the CVIs, except WSJI, failed to detect the actual cluster number of the image.

Figure 4e–h provides the clustering results of HYDICE data with the cluster number  $K = 3, 4, 5, 6$ , of which the clustering with  $K = 4$  properly separated the four ground truth classes (roads, trees, trail, and grass) (Figure 4f). In the case of clustering with  $K = 3$ , there were clear errors due to the incorrect merging of trees and roads (Figure 4e). However, it was still suggested by half of the CVIs, including DBI, MPC, XBI, KI, CWBI, TI, PBMFI, and WLI (Table 9). Similar to the experiment on Hyperion, WSJI was the only index returning the correct information about cluster number.

Figure 4i–l lists the clustering results of ROSIS data with the cluster number  $K = 3, 4, 5, 6$ . Among them, the clustering with  $K = 5$  successfully classified the five ground truth classes (meadows, trees, asphalt, bricks, and shadows) (Figure 4k). For the case of  $K = 3$ , trees and shadows were not distinguished (Figure 4i). However, this incorrect suggestion was also made by as many as half of the CVIs, including DBI, CHI, MPC, XBI, KI, TI, CWBI, and WLI (Table 10). Once again, only WSJI correctly indicated the actual cluster number of the image.

Figure 4m–p shows the clustering results of AVIRIS data with the cluster number  $K = 3, 4, 5, 6$ , in which the five ground truth classes (vineyard untrained, celery, fallow smooth, fallow plow, and stubble) were well classified with  $K = 5$  (Figure 4o). However, no CVI was able to indicate the actual cluster number of the image (Table 11). Instead, most of them (DBI, DI, PC, MPC, XBI, KI, TI, CWBI, WSJI, and WLI) preferred four clusters for the image, which merged the classes of fallow smooth and fallow plow (Figure 4n).

Figure 5 illustrates the percentage of successes (correct guesses) achieved by the 16 CVIs. Table 12 summarizes the cluster validity results of the 16 CVIs by FCM on nine types of remote sensing image datasets, in which the actual cluster number of each image is listed in column K# while those indicated by CVIs are shown in other columns. From the table it can be seen that WSJI was the only index that correctly recognized the actual cluster numbers of all of the datasets (including multispectral and hyperspectral data), except for the AVIRIS image. Thus WSJI, was the most effective and stable index of all. CHI and FSI succeeded in multispectral datasets but failed in hyperspectral datasets. The DBI, DI, MPC, SCI, XBI, KI, TI, CWBI, and WLI indices were only effective for two multispectral images. CVIs including PC, PE, and PBMFI failed, generally, except for the simple QuickBird experiment. SVFI failed for all images.



**Figure 5.** The overall performance of CVIs by applying FCM algorithm to cluster nine types of remote sensing datasets.

**Table 12.** The optimal cluster numbers indicated by the CVIs by FCM for each remote sensing image.

Images	K#	PC	PE	MPC	DBI	DI	CHI	FSI	SCI
Multispectral image									
QuickBird	3	3*	3*	3*	3*	3*	8	8	8
Landsat TM	4	2	2	2	2	7	4*	4*	4*
Landsat ETM+	4	3	2	2	2	5	4*	3	7
GaoFen-1	5	2	2	5*	5*	2	5*	5*	5*
FLC1	5	2	2	3	2	5*	5*	5*	6
Hyperspectral image									
Hyperion	4	2	2	2	2	10	5	6	10
HYDICE	4	2	2	3	3	8	5	6	6
ROSIS	5	4	2	4	4	4	8	6	10
AVIRIS	5	2	2	3	3	4	3	6	10
Images	C	XBI	KI	TI	CWBI	WSJI	PBMFI	SVFI	WLI
Multispectral image									
QuickBird	3	3*	3*	3*	3*	3*	3*	10	3*
Landsat TM	4	2	2	2	4*	4*	2	8	2
Landsat ETM+	4	2	2	2	2	4*	2	10	2
GaoFen-1	5	5*	5*	5*	3	5*	2	7	5*
FLC1	5	3	3	3	3	5*	2	10	2
Hyperspectral image									
Hyperion	4	2	2	2	2	4*	3	10	3
HYDICE	4	3	3	3	3	4*	3	9	3
ROSIS	5	3	3	3	3	5*	2	10	3
AVIRIS	5	4	4	4	4	4	2	7	4

Note: K# in the second column denotes the actual cluster numbers of the images, \* denotes that the actual cluster number of the image was correctly identified by the index.

Table 13 summarizes the cluster validity results of the 16 CVIs by K-means on the remote sensing images. As expected, the results are similar to those by FCM: WSJI performed the best for both multispectral and hyperspectral images, followed by CHI and FSI, both of which were effective for most multispectral images; the DBI, DI, MPC, SCI, XBI, KI, TI, CWBI, and PBMFI performed worse than the above-mentioned CVIs, with correct identification of cluster numbers for only one or two multispectral images; PC, PE, and SVFI behaved the worst since they failed for all images.

**Table 13.** The optimal cluster numbers indicated by the CVIs by K-means for each remote sensing image.

Images	K#	PC	PE	MPC	DBI	DI	CHI	FSI	SCI
Multispectral image									
QuickBird	3	2	2	3*	3*	3*	9	7	7
Landsat TM	4	2	2	2	2	8	4*	4*	4*
Landsat ETM+	4	2	2	2	2	9	4*	4*	9
GaoFen-1	5	2	2	5*	5*	2	5*	5*	5*
Hyperspectral image									
Hyperion	4	2	2	2	2	7	5	5	7
HYDICE	4	2	2	3	3	7	7	7	5
ROSIS	5	2	2	3	3	4	3	9	9
AVIRIS	5	2	2	3	3	4	3	6	10
Images	C	XBI	KI	TI	CWBI	WSJI	PBMFI	SVFI	WLI
Multispectral image									
QuickBird	3	3*	3*	3*	3*	3*	3*	10	2
Landsat TM	4	2	2	2	2	4*	2	10	2
Landsat ETM+	4	2	2	2	3	4*	2	10	2
GaoFen-1	5	5*	5*	5*	5*	5*	2	9	5*
Hyperspectral image									
Hyperion	4	2	2	2	2	4*	3	10	2
HYDICE	4	5	5	5	3	4*	2	10	3
ROSIS	5	6	6	6	3	5*	2	10	3
AVIRIS	5	4	4	4	4	4	2	7	4

Note: \* denotes that the actual cluster number of the image was correctly identified by the index; results on FLC1 image were not included in the table in consideration of the relative lower classification accuracy.

## 5. Discussion

In essence, a CVI is designed to measure the degree of compactness and/or separation of clusters. However, the two indicators are potentially in conflict because the number of clusters is generally positively associated with compactness, but negatively with separation. Thus, a balanced definition of compactness and separation is crucial to the designing of CVIs. Most CVIs measure compactness in a similar way, *i.e.*, the distance between each data point and its cluster center. The major differences among CVIs, thus, lie in whether the indicator of separation is utilized and how it is defined. In fact, separation is not included in simple CVIs, whereas it is explicitly presented in all the advanced CVIs but with non-uniform definitions, *e.g.*, the minimum or maximum distance between clusters. Beside issues of measuring compactness and separation, the performance of CVIs is also closely related to the nature of the experimental datasets. For remote sensing data, significant overlaps among clusters often exist [15]. This property of the datasets must, therefore, be considered by CVIs.

In our experiments, simple CVIs like PC, PE, and MPC were the worst performers. They underestimated the cluster numbers of most images (Table 10), consistent with previous studies [12,20]. This is mainly because they are built on the assumption that clusters are dispersed far away from each other, and the belonging (membership) of each point to its cluster is much larger than it is to other clusters. This assumption is, however, not necessarily valid in the context of the fuzzy property of remote sensing data. Thus, those CVIs without separation indicators are incapable of effectively handling such complex datasets.

Some advanced CVIs (including DBI, DI, XBI, KI, TI, PBMFI, SVFI, and WLI) usually performed better than simple CVIs, but were still far from satisfactory. This is mainly because these CVIs take the minimum distance (*e.g.*, DBI and XBI) or the maximum distance (*e.g.*, PBMFI) between clusters to measure separation and this results in a preference for clustering in which clusters are dispersed as far as possible [12]. However, clusters in remote sensing data are usually allocated closely. Those CVIs, in which separation exerts a great impact, therefore, underestimate the actual cluster numbers of the images (Table 10). It was found that some advanced CVIs (CHI, FSI, and SCI), in which the distance between each cluster center to the global center was taken as separation, worked better than the CVIs above. The separation measured with the distance from a single cluster to the global center, rather than the extreme (*i.e.*, the minimum or maximum) distance between clusters, permits the existence of some clusters with close distances. However, they also failed in all experiments for hyperspectral images. The small distance between clusters in hyperspectral data weakened the role of separation in these CVIs, but enhanced the impact of compactness, thereby tending to overestimate the cluster number (Table 10).

Obviously, the bottleneck of most existing CVIs in handling large scale data (such as remote sensing data) lies in how to balance the two conflicting factors (compactness and separation) to correctly indicate the actual cluster number of the data. Fortunately, WSJI (the only index) strikes the right balance between the two factors through normalization [13], and its effectiveness is clearly verified in our experiments. This is especially suitable for handling complex remote sensing datasets: if the cluster number is underestimated, a large compactness emerges to penalize the clustering with too few clusters; conversely, if the cluster number is overestimated, a large separation appears to penalize the clustering with too many clusters; it is only when the actual cluster number is defined that both compactness and separation simultaneously become relatively small. The WSJI seemed to indicate a non-optimal clustering ( $K = 4$ ) only in the AVIRIS experiment, in which fallow smooth and fallow plow were merged into one cluster (Figure 4n). This is because the between-cluster distance of the two classes was small (having similar spectral characteristics (Figure 2l)), the value of separation increased significantly, so the WSJI did not indicate the optimal clustering ( $K = 5$ ). However, it was found that the two classes essentially belonged to the same land cover class (fallow), only differing in the surface roughness of the ground (smooth or plowed). In this sense, WSJI still detected the “real” cluster number of the image.

It should be noted that CVIs, a post-processing procedure applied to clustering, is based on the assumption that the structure of the dataset is well described by the cluster methods [35]. Otherwise, the evaluation would be meaningless [44]. Fortunately, the clustering results generated by the FCM algorithm worked fairly well in our experiments, as indicated by our land cover maps, although the cluster numbers were not very large. This is mainly due to the fact that it is difficult for FCM to handle complex images with a larger number of clusters [45,46]. In the future, it would be worthwhile to investigate more sophisticated methods (e.g., artificial intelligence-based algorithms) for image clustering. In addition to the 16 CVIs included in the experiments, some types of CVIs (such as graph-based validity measures [47]) that have recently appeared in the field of pattern recognition could be explored in further research to test their effectiveness in the area of remote sensing.

There was one dataset for each RS sensor in our experiment because of the length limitation of the paper. However, some remote sensing images, such as QuickBird *versus* Gaofen-1, and HYDICE *versus* AVIRIS, have great similarities in terms of number of bands, spatial resolution, and spectral wavelength. Two similar images can, thus, be confidently seen as two scenes of images acquired by effectively the same sensor. It is noted that the images employed in our experiments were acquired at different locations, which allows us to analyze the performance of CVIs on various types of landscapes (e.g., farmland, marsh and urban). Obviously, this might be helpful for the generalization of conclusions drawn in this paper.

## 6. Conclusions

In this paper, we evaluated the effectiveness of 16 representative CVIs on nine types of remote sensing datasets by utilizing the FCM algorithm for image clustering. From the experimental results, it was found that, due mainly to inappropriate definitions of separation, most existing CVIs were not suitable for remote sensing datasets (especially for hyperspectral data), which usually have significant overlaps between clusters. The only effective index was the WSJI, which indicated the real cluster numbers of the images (with either multispectral or hyperspectral data), because of its balanced combination between compactness and separation through normalization. This index, thus, deserves to be given first priority for future remote sensing classification applications. However, we do not claim that it would be effective in all applications because of the complexity of remote sensing datasets (e.g., a variety of formats, spatial scales, and spectral scales, among others). Furthermore, the selected algorithms and their operational parameters are very important for the performance of CVI, as they directly control the clustering quality (classification accuracy) of the image. In addition, the land use/cover classes covered by the images may also impact the cluster validity results. For example, WSJI failed in the AVIRIS experiment due to the very similar spectral characteristics of the two fallow classes (fallow smooth and fallow plow). As stated by Pal and Bezdek [48] “no matter how good your index is, there is a data set out there waiting to trick it (and you)”.

**Acknowledgments:** This work was supported by the National Natural Science Foundation of China (grant number: 41301465, 41271196), the National Major Program of China (grant number: 21-Y30B05-9001-13/15-2) and the “12th Five-Year Plan” Wetland and Blackland Specialised Databases Program of the Chinese Academy of Sciences (grant number: XXH12504-3-03). The authors would like to thank P. Gamba for providing the University of Pavia ROSIS data sets, and D. Landgrebe for providing the Washington DC HYDICE data sets. We thank the anonymous reviewers for their constructive comments.

**Author Contributions:** Huapeng Li conceived and designed the experiments; Huapeng Li and Xiaohui Ding performed the experiments; Huapeng Li, Shuqing Zhang and Ce Zhang analyzed the experimental results; Huapeng Li, Shuqing Zhang and Patricia Dale wrote the paper.

**Conflicts of Interest:** The authors declare no conflict of interest.

## References

1. Kerr, J.T.; Ostrovsky, M. From space to species: Ecological applications for remote sensing. *Trends Ecol. Evol.* **2003**, *18*, 299–305. [[CrossRef](#)]

2. Lu, D.; Weng, Q. A survey of image classification methods and techniques for improving classification performance. *Int. J. Remote Sens.* **2007**, *28*, 823–870. [[CrossRef](#)]
3. Otukey, J.R.; Blaschke, T. Land cover change assessment using decision trees, support vector machines and maximum likelihood classification algorithms. *Int. J. Appl. Earth Obs. Geoinf.* **2010**, *12*, S27–S31. [[CrossRef](#)]
4. Loveland, T.R.; Reed, B.C.; Brown, J.F.; Ohlen, D.O.; Zhu, Z.; Yang, L.; Merchant, J.W. Development of a global land cover characteristics database and IGBP DISCover from 1 km AVHRR data. *Int. J. Remote Sens.* **2000**, *21*, 1303–1330. [[CrossRef](#)]
5. Friedl, M.A.; McIver, D.K.; Hodges, J.C.F.; Zhang, X.Y.; Muchoney, D.; Strahler, A.H.; Woodcock, C.E.; Gopal, S.; Schneider, A.; Cooper, A.; et al. Global land cover mapping from MODIS: Algorithms and early results. *Remote Sens. Environ.* **2002**, *83*, 287–302. [[CrossRef](#)]
6. Xiao, X.M.; Boles, S.; Liu, J.Y.; Zhuang, D.F.; Liu, M.L. Characterization of forest types in Northeastern China, using multi-temporal SPOT-4 VEGETATION sensor data. *Remote Sens. Environ.* **2002**, *82*, 335–348. [[CrossRef](#)]
7. Schmid, T.; Koch, M.; Gumuzzio, J.; Mather, P.M. A spectral library for a semi-arid wetland and its application to studies of wetland degradation using hyperspectral and multispectral data. *Int. J. Remote Sens.* **2004**, *25*, 2485–2496. [[CrossRef](#)]
8. Duda, T.; Canty, M. Unsupervised classification of satellite imagery: Choosing a good algorithm. *Int. J. Remote Sens.* **2002**, *23*, 2193–2212. [[CrossRef](#)]
9. Bandyopadhyay, S.; Maulik, U. Genetic clustering for automatic evolution of clusters and application to image classification. *Pattern Recognit.* **2002**, *35*, 1197–1208. [[CrossRef](#)]
10. Wang, W.N.; Zhang, Y.J. On fuzzy cluster validity indices. *Fuzzy Set Syst.* **2007**, *158*, 2095–2117. [[CrossRef](#)]
11. Halkidi, M.; Batistakis, Y.; Vazirgiannis, M. On clustering validation techniques. *J. Intell. Inf. Syst.* **2001**, *17*, 107–145. [[CrossRef](#)]
12. Wu, C.H.; Ouyang, C.S.; Chen, L.W.; Lu, L.W. A new fuzzy clustering validity index with a median factor for centroid-based clustering. *IEEE Trans. Fuzzy Syst.* **2014**, *23*, 701–718. [[CrossRef](#)]
13. Sun, H.J.; Wang, S.R.; Jiang, Q.S. FCM-based model selection algorithms for determining the number of clusters. *Pattern Recognit.* **2004**, *37*, 2027–2037. [[CrossRef](#)]
14. Das, S.; Abraham, A.; Konar, A. Automatic clustering using an improved differential evolution algorithm. *IEEE Trans. Syst Man Cybern. A* **2008**, *38*, 218–237. [[CrossRef](#)]
15. Maulik, U.; Saha, I. Automatic fuzzy clustering using modified differential evolution for image classification. *IEEE Trans. Geosci. Remote Sens.* **2010**, *48*, 3503–3510. [[CrossRef](#)]
16. Zhong, Y.F.; Zhang, S.; Zhang, L.P. Automatic fuzzy clustering based on adaptive multi-objective differential evolution for remote sensing imagery. *IEEE J. Sel. Top. Appl. Earth Observ. Remote Sens.* **2013**, *6*, 2290–2301. [[CrossRef](#)]
17. Ma, A.L.; Zhong, Y.F.; Zhang, L.P. Adaptive multiobjective memetic fuzzy clustering algorithm for remote sensing imagery. *IEEE Trans. Geosci. Remote Sens.* **2015**, *53*, 4202–4217. [[CrossRef](#)]
18. Bandyopadhyay, S.; Pal, S.K. Pixel classification using variable string genetic algorithms with chromosome differentiation. *IEEE Trans. Geosci. Remote Sens.* **2011**, *39*, 303–308. [[CrossRef](#)]
19. Rezaee, M.R.; Lelieveldt, B.P.F.; Reiber, J.H.C. A new cluster validity index for the fuzzy c-mean. *Pattern Recognit. Lett.* **1998**, *19*, 237–246. [[CrossRef](#)]
20. Pakhira, M.K.; Bandyopadhyay, S.; Maulik, U. A study of some fuzzy cluster validity indices, genetic clustering and application to pixel classification. *Fuzzy Sets Syst.* **2005**, *155*, 191–214. [[CrossRef](#)]
21. Arbelaitz, O.; Gurrutxaga, I.; Muguerza, J.; Perez, J.M.; Perona, I. An extensive comparative study of cluster validity indices. *Pattern Recognit.* **2013**, *46*, 243–256. [[CrossRef](#)]
22. Bezdek, J.C. *Partition Recognition with Fuzzy Objective Function Algorithms*; Plenum Press: New York, NY, USA, 1981.
23. Bezdek, J.C. *Partition Structures: A Tutorial in the Analysis of Fuzzy Information*; CRC Press: Boca Raton, FL, USA, 1987.
24. Cai, W.L.; Chen, S.C.; Zhang, D.Q. Fast and robust fuzzy c-means clustering algorithms incorporating local information for image segmentation. *Pattern Recognit.* **2007**, *40*, 825–838. [[CrossRef](#)]
25. Bezdek, J.C. Cluster validity with fuzzy sets. *J. Cybern.* **1974**, *3*, 58–72. [[CrossRef](#)]
26. Dave, R.N. Validating fuzzy partition obtained through c-shells clustering. *Pattern Recognit. Lett.* **1996**, *17*, 613–623. [[CrossRef](#)]

27. Davies, D.L.; Bouldin, D.W. A clustering separation measure. *IEEE Trans. Pattern Anal. Mach. Intell.* **1979**, *1*, 224–227. [[CrossRef](#)] [[PubMed](#)]
28. Dunn, J.C. A fuzzy relative of the ISODATA process and its use in detecting compact well-separated clusters. *J. Cybern.* **1973**, *3*, 32–57. [[CrossRef](#)]
29. Calinski, T.; Harabasz, J. A dendrite method for cluster analysis. *Commun Stat. Theory Methods* **1974**, *3*, 1–27. [[CrossRef](#)]
30. Fukuyama, Y.; Sugeno, M. A new method of choosing the number of clusters for fuzzy c-means method. In Proceedings of the 5th Fuzzy System Symposium, Kobe, Japan, 2–3 June 1989.
31. Xie, X.L.; Beni, G. A validity measure for fuzzy clustering. *IEEE Trans. Pattern Anal.* **1991**, *13*, 841–847. [[CrossRef](#)]
32. Kwon, S.H. Cluster validity index for fuzzy clustering. *Electron. Lett.* **1998**, *34*, 2176–2177. [[CrossRef](#)]
33. Tang, Y.G.; Sun, F.C.; Sun, Z.Q. Improved validation index for fuzzy clustering. In Proceedings of the American Control Conference, Portland, OR, USA, 8–10 June 2005.
34. Zahid, N.; Limouri, N.; Essaid, A. A new cluster-validity for fuzzy clustering. *Pattern Recognit.* **1999**, *32*, 1089–1097. [[CrossRef](#)]
35. Zalik, K.R.; Zalik, B. Validity index for clusters of different sizes and densities. *Pattern Recognit. Lett.* **2011**, *32*, 221–234. [[CrossRef](#)]
36. Jain, A.K. Data clustering: 50 years beyond K-means. *Pattern Recognit. Lett.* **2010**, *31*, 651–666. [[CrossRef](#)]
37. Wang, L.; Sousa, W.P.; Gong, P.; Biging, G.S. Comparison of IKONOS and QuickBird images for mapping mangrove species on the Caribbean coast of Panama. *Remote Sens. Environ.* **2004**, *91*, 432–440. [[CrossRef](#)]
38. Li, J.; Chen, X.L.; Tian, L.Q.; Huang, J.; Feng, L. Improved capabilities of the Chinese high-resolution remote sensing satellite GF-1 for monitoring suspended particulate matter (SPM) in inland waters: Radiometric and spatial considerations. *ISPRS J. Photogramm. Remote Sens.* **2015**, *106*, 145–156. [[CrossRef](#)]
39. Tadjudin, S.; Landgrebe, D.A. Robust parameter estimation for mixture model. *IEEE Trans. Geosci. Remote Sens.* **2000**, *38*, 439–445. [[CrossRef](#)]
40. Ham, J.; Chen, Y.C.; Crawford, M.M.; Ghosh, J. Investigation of the random forest framework for classification of hyperspectral data. *IEEE Trans. Geosci. Remote Sens.* **2005**, *43*, 492–501. [[CrossRef](#)]
41. Yin, J.H.; Wang, Y.F.; Hu, J.K. A new dimensionality reduction algorithm for hyperspectral image using evolutionary strategy. *IEEE Trans. Ind. Inform.* **2012**, *8*, 935–943. [[CrossRef](#)]
42. Li, J.; Bioucas-Dias, J.M.; Plaza, A. Spectral-spatial hyperspectral image segmentation using subspace multinomial logistic regression and markov random fields. *IEEE Trans. Geosci. Remote Sens.* **2012**, *50*, 809–823. [[CrossRef](#)]
43. Zhou, Y.C.; Peng, J.T.; Chen, C.L.P. Extreme learning machine with composite kernels for hyperspectral image classification. *IEEE J. Selected Topics Appl. Earth Observ. Remote Sens.* **2015**, *8*, 2351–2360. [[CrossRef](#)]
44. Kim, D.W.; Lee, K.H.; Lee, D.H. On cluster validity index for estimation of the optimal number of fuzzy clusters. *Pattern Recognit.* **2004**, *37*, 2009–2025. [[CrossRef](#)]
45. Maulik, U.; Bandyopadhyay, S. Fuzzy partitioning using a real-coded variable-length genetic algorithm for pixel classification. *IEEE Trans. Geosci. Remote Sens.* **2003**, *41*, 1075–1081. [[CrossRef](#)]
46. Paoli, A.; Melgani, F.; Pasolli, E. Clustering of hyperspectral images based on multiobjective particle swarm optimization. *IEEE Trans. Geosci. Remote Sens.* **2009**, *47*, 4175–4188. [[CrossRef](#)]
47. Ilc, N. Modified Dunn’s cluster validity index based on graph theory. *Electr. Rev.* **2012**, *2*, 126–131.
48. Pal, N.R.; Bezdek, J.C. Correction to “on cluster validity for the fuzzy c-means model”. *IEEE Trans. Fuzzy Syst.* **1997**, *5*, 152–153. [[CrossRef](#)]

